CNTs/SnO_2 AND CNTs/MnO_2 NANOCOMPOSITES FOR THE FABRICATION OF THE ELECTRODES FOR SUPERCAPACITORS

(Date received: 10.05.12/Date accepted: 09.11.12)

Ir. Dr Ng Kok Chiang*[1], Dr Daniel Jewell[2]

[1]MyBig Sdn. Bhd., No. 1, Jalan P4/7, Seksyen 4, Bandar Teknologi Kajang, 43500 Semenyih, Selangor, Malaysia.
[2]Department of Materials Science and Metallurgy, New Museums Site, Pembroke Street, University of Cambridge, Cambridge CB2 3QZ, United Kingdom.
*E-mail: [1]*kokchiang.ng@leonghing.com*

ABSTRACT

The development of next generation high-energy and high-power aqueous supercapacitors is vital in an era when power demand has peaked. In terms of engineering related issues at the micro level, the major area urgently requiring attention is the development of new nanocomposite materials. This article reports on nanocomposites which demonstrate superiority in terms of three-dimensional structure and which possess electrical conductivity equivalent to metallic conductors as a result of CNTs which complement the high redox-active properties of the transition metal oxides. Such combined contributions, when applied in supercapacitors, lead to increased charge storage capabilities and exceptional cycling stability. Two nanocomposites, namely, CNTs/SnO_2 and CNTs/MnO_2, were synthesised their physicochemical properties examined by X-ray diffraction, scanning electron microscopy, cyclic voltammetry and galvanostatic charge-discharge. The nanocomposites show superior results in terms of charge-storage mechanisms, cycle life, and electrochemical kinetics. Uniquely, in this paper, CNTs/SnO_2 nanocomposites were also reported as an alternative negative electrode material to the commonly used activated carbon in asymmetrical supercapacitors.

Keywords: *Energy Storage, Fabrication, Nanocomposites, Supercapacitors*

1.0 INTRODUCTION

Energy efficient and robust power devices are key to overcoming the daunting challenges of climate change and the depletion of the earth's fossil fuels. As a result of an extensively diversified and globalised energy market, electrochemical capacitors, which are also known as supercapacitors, are becoming one of the vital energy-storage devices of the 21st century. This is because electrochemical capacitors bridge the crucial performance disparity between high energy-density fuel cells or batteries and high power-density traditional capacitors. The necessary developmental advances can be achieved through innovations in pseudo-capacitive nanocomposites of transition metal oxides and carbon nanotubes (CNTs) which combine both ion adsorptions (interfacial capacitance) and fast redox reactions (pseudo-capacitance) for energy storage.

In addition to enhancing the core performance of supercapacitors, there is also a need to develop materials which offer an alternative to activated carbon as a negative electrode material in asymmetric aqueous electrochemical capacitors. There have already been many studies of probable positive electrode materials for supercapacitors, especially those with very good pseudo-capacitive properties as they are able to outperform the traditional electrical-double layer storage mechanism. The simple logic therefore is to search for a low cost metal oxide that is active in the negative potential range, such as tin oxide (SnO_2) which has been examined extensively as the negative electrode material in lithium ion batteries [1-4]. Lithium ion battery research has already progressed to combining SnO_2 [5, 6] and CNTs as a promising anode candidate, owing to the excellent mechanical and electrical properties of CNTs [7-9], SnO_2 has only recently been studied in supercapacitors as the positive electrode material [5-9].

In order to address these separate challenges, two different nanocomposite materials have been synthesised. In the case of core performance improvement, a carbon nanotube manganese oxide nanocomposite (denoted CNTs/MnO_2) was synthesised by the redox deposition method[1]. In this approach $KMnO_4$ was used as an oxidant which would react with the CNTs, to be reduced to an insoluble form of MnO_2 in an aqueous solution. This precipitate then anchors itself onto the surface of the CNTs to form the CNTs/MnO_2 nanocomposite [10-14]. Such composites were previously reported to exhibit very high electrode specific capacitance (≥ 5.0 F/cm^2) in the positive potential range [10].

For the production of a new negative electrode material for aqueous asymmetric supercapacitors, a nanocomposite of carbon nanotubes and tin oxide (denoted CNTs/SnO_2) was synthesised in which tin oxides were coated on the surface of individual CNTs. Good understanding of the science of materials is important for practicing engineers to fully comprehend the nature, capabilities, and ratings of energy devices that are increasingly being built with these advanced nanocomposite materials.

2.0 METHODOLOGY

CNTs/MnO_2 nanocomposite synthesis – The CNTs/MnO_2 nanocomposite was synthesised via spontaneous redox deposition of MnO_2 on the CNTs in the $KMnO_4$ aqueous solution as previously reported[2]. In this synthesis, one gram of $KMnO_4$

(Fluka ≥99.0% (RT)) was dissolved in 50.0 mL of deionised water in an Erlenmeyer flask before the addition of acid-treated CNTs (to form a nanocomposite of CNTs/MnO_2 of 4:6 w/w). The resulting mixture was continuously stirred for nine days in the covered flask until the purple colour disappeared. During and after the reaction, clear solutions gradually appeared with the product settling to the bottom of the flask. The resulting nanocomposite was filtered, washed and dried in the oven overnight at 60˚C.

CNTs/SnO_2 nanocomposite synthesis – In the synthesis of the CNTs/SnO_2, 1.0 g of tin (II) chloride dihydrate (Fisher 97+%) was dissolved in 50.0 mL of deionised H_2O in an Erlenmeyer flask and 1.0 mL of HCl (38%) was added and stirred continuously for 1.0 hour to dissolve the tin (II) chloride. Then, the acid-treated CNTs were added to the solution and stirred for 24 hours at room temperature to form a nanocomposite of CNTs/SnO_2 of 4:6 w/w. The resulting mixture was then filtered, washed and dried overnight at 60˚C in a conventional oven.

Chemical and structural characterizations – The nanocomposites, all in the powder form, were characterized by X-ray diffraction (XRD, Hiltonbrooks DG3 generator plus Philips PW1050/25 goniometer, CuKα radiation), an environmental scanning electron microscope (SEM, Philips FEI XL30 FEG-ESEM), a low resolution TEM (LR-TEM, JEOL 2000FX), and a high resolution TEM (HRTEM, JEOL 2100F).

Preparation of the electrode and electrochemical analysis – The nanocomposite (34.2 mg) with a binder (3.0 mg, 60% w.t. aqueous emulsion of polytetrafluoroethylene, PTFE, Aldrich) was thoroughly dispersed in 4.0 mL of deionised water. The mixture (10.0 µL, with 0.0855 mg of the nanocomposite) was drop-cast onto a graphite disc working electrode (0.5 cm in diameter) using an electronic micropipette (EDP3 Rainin LTS, 10-100 µL, with wide orifice tips). Upon evaporation, the resulting thin film (13.44 µm on average thickness) on the electrode was dried in a desiccator overnight before electrochemical tests (AUTOLAB PGSTAT30) in a one-compartment three-electrode cell with the Ag/AgCl (3.0 M KCl) reference electrode and a graphite counter electrode at room temperature.

3.0 RESULTS AND DISCUSSIONS

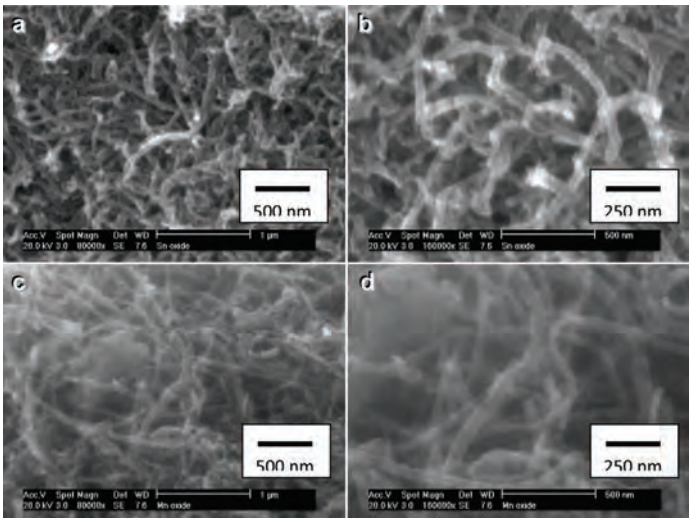

Figure 1: SEM images of the nanocomposites at different magnifications, i.e. 80,000x and 160,000x (a, b) CNTs/SnO_2 and (c, d) CNTs/MnO_2

Figure 1 shows the SEM images of the acid-treated CNTs after SnO_2 (a, b) and MnO_2 deposition (c, d) at two magnifications as indicated. The images of the CNTs/SnO_2 and CNTs/MnO_2 nanocomposites show that they retained the bundle nature and the three-dimensional entangled structures originating from the as-received CNTs. This shows that the SnO_2 and MnO_2 deposits did not block the opening and the porous structure which is inherent to the CNTs. The porosity can be observed as the dark spots in Figure 1 which are also the spaces created due to the nature of the CNTs. Maintaining such configurations assists the movement of the ions into and out of the positive and negative electrodes of the nanocomposites as mentioned previously. The SEM images of the nanocomposites demonstrate that thin coatings of the metal oxides exist around the CNTs. The jagged and consistent coarse surfaces, especially for the CNTs/SnO_2 nanocomposite, illustrate the evenly distributed SnO_2 on the surface of individual CNTs throughout the structure. The coating can only be further confirmed and substantiated by TEM images in Figure 2, 3, and 4 in the subsequence sections.

As for the SEM analysis, the TEM images of the overall CNTs/SnO_2 60% w.t. confirmed that the nanocomposite retained the bundle nature of the CNTs as can be seen in Figure 2(a). It is noted that almost all the CNTs or CNT bundles in the sample are individually coated with thin and uniform layers of SnO_2. Enlarging the image of the end of one of the nanocomposite's fibrils reveals a very thin coating of nanocrystalline SnO_2 of about 5 nm width as can be observed in Figure 2(d). This also demonstrates the nature of the open-ended CNT the fact that the nanocrystalline SnO_2 is coated onto the CNT even to the very tip. It is also notable, as shown from the bundle in Figure 2(a), that separate SnO_2 agglomerates (away from the CNTs) were not seen. Instead, the SnO_2 nano-grains nucleate only on the surface of the CNTs. Finally, it can be observed that the CNT's walls and cavities are only vaguely visible in Figure 2(a-c) which may be due to the interference of thicker oxide coatings that made it difficult to resolve the structures by TEM [10].

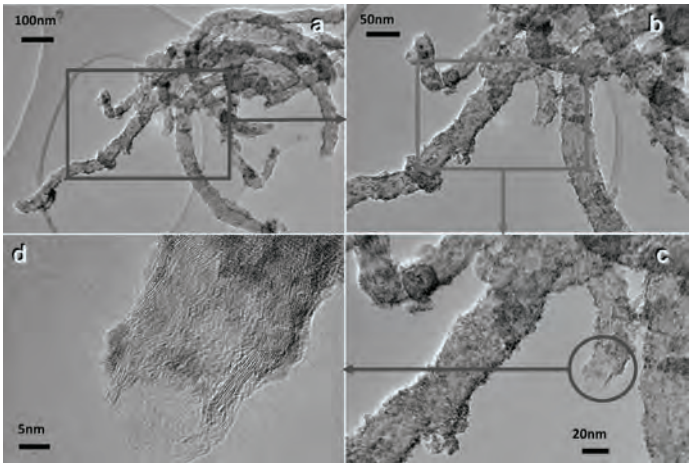

Figure 2: TEM images of the CNTs/SnO_2 60% w.t. nanocomposite; (a) and (b) overviews of the fully SnO_2-coated CNTs, (c) and (d) TEM images of enlarged micrographs depicting the open-ended tube of a CNT coated with a nanocrystalline coating SnO_2

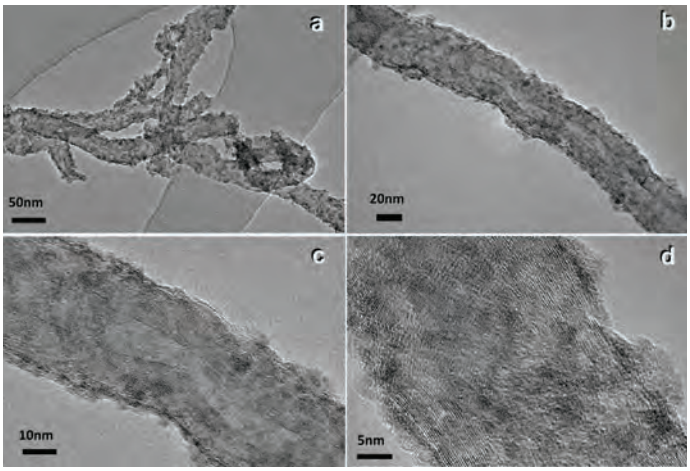

Figure 3: Closed-up examination of various other strands of the coated CNTs/SnO_2 60% w.t. nanocomposite; (a) tangled SnO_2 coated CNTs, (b) and (c) a mid-portion of the nanocomposite fibril coated with SnO_2 and (d) densely coated with nanocrystalline particles of SnO_2 on the surface of the CNT

Figure 3(a) shows more strands of CNTs coated uniformly with SnO_2 throughout. Figure 3(b, c) present typical TEM images of mid portions of SnO_2 coated CNTs where the parallel and long fringes are from the CNT walls (the grapheme layers) are clearly distinguishable from those almost randomly originated from the nanocrystalline SnO_2. It should also be noted that the structure of the CNTs remain intact. No corrosion was observed in the deposition of SnO_2 onto the CNT as compared to that caused by the $KMnO_4$ in the deposition of MnO_2 onto the CNTs. This can be clearly seen in the bundled nanocomposites in Figure 3 (a, b) and the long nanocomposite fibril in Figure 3(b) as well as the deposition of SnO_2 at the very end of the CNT in Figure 3(d). Such preservation of the CNTs structure may be attributed to the fact that SnO_2 deposition resulted from the reaction between the Sn^{2+} ion and an oxidant, such as dissolved oxygen gas in the synthesis solution, without attacking the CNTs [15]. In Figure 3(d), on the enlarged portion of one of the nanocomposite fibrils the observed SnO_2 nanoparticles are rounded with diameters of about 4 nm and are distributed evenly on the surface of the CNT. These SnO_2 nanoparticulates also densely populate the CNT surface and show fringes on each of them, confirming nanocrystallinity.

Figure 4(a) shows the overview of the well-dispersed CNTs/MnO_2 60%w.t. nanocomposite on the carbon-holey grids examined under the TEM. In all the TEM images of the CNTs/MnO_2 60% w.t. nanocomposite, the surfaces of the CNTs are well covered with MnO_2 deposits. Figure 4(c) and (d) depict uneven depositions of nano-layers of MnO_2 on the CNTs while (e) and (f), enlarged views, show that the CNT walls remained intact even with the presence of the thick layer of MnO_2 on the surface of the CNT. It was previously reported that the mechanism behind the deposition results in the formation of thick MnO_2 coatings on the CNTs [10, 11].

In short, the growth of MnO_2 continues even after the surface of the CNTs are fully covered with MnO_2 deposit in accordance with the 'MEC' (microelectrochemical cell) principle, i.e. electrons are moved from the defect sites of the CNTs to other sites in contact with MnO_4^- where the anion is reduced to MnO_2 as in any electrodeposition process. Thus, the thick coating and no separated precipitation from the CNT structure is observed. Figure 4(b) and (d) also show the broken and short-ended characteristics of the CNT indicating that corrosion by $KMnO_4$ in the reduction to the insoluble MnO_2 might have taken place. The layered structure of the MnO_2 as can be seen in the enlarged TEM images of (e) and (f), would be excellent for retaining the facile transport pathways for both protons and electrons [16] as in the case of ruthenium dioxide, according to the following reaction (1) [11, 17-20]:

$$MnO_x(OH)_y + \delta H^+ + \delta^+ \rightleftharpoons MnO_{x-\delta}(OH)_{y+\delta} \quad (1)$$

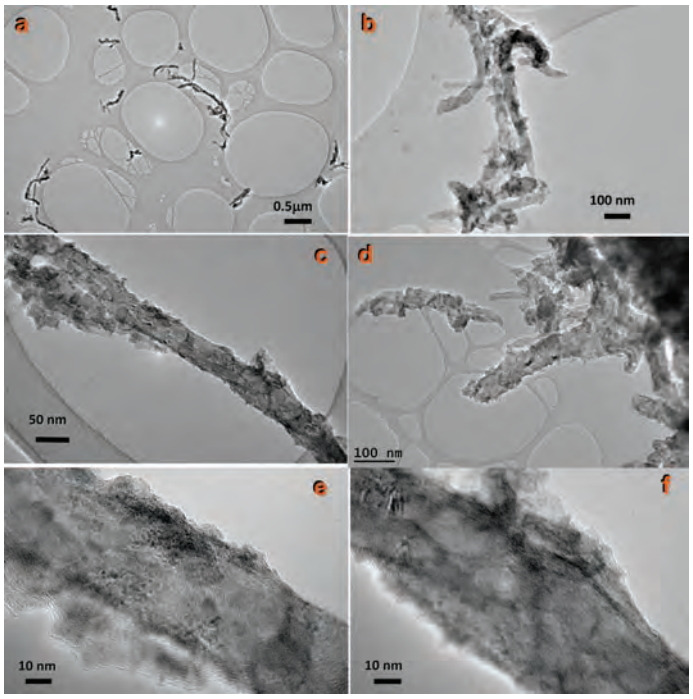

Figure 4: TEM images of the CNTs/MnO_2 60% w.t. nanocomposite

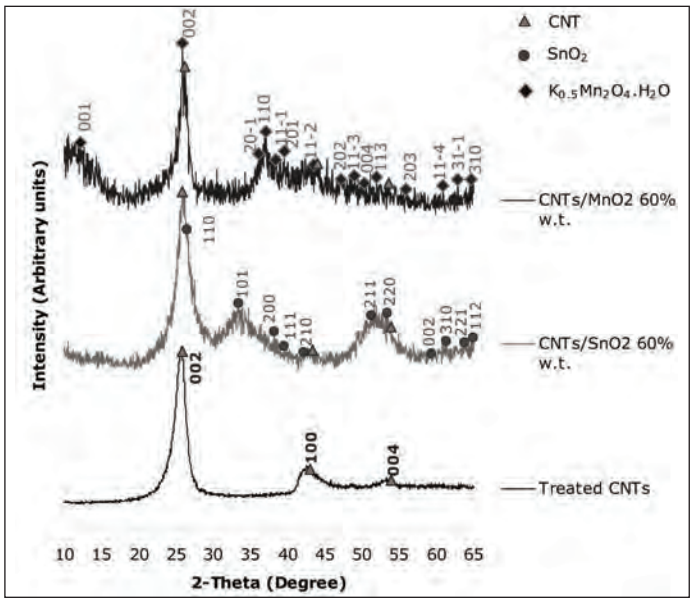

Figure 5: XRD spectrum of the nanocomposites and the acid-treated CNTs

The XRD patterns of the nanocomposites reveal the presence of cassiterite-type SnO_2 (JCPDS 41-1445) in the CNTs/SnO_2 60% w.t. nanocomposite. The broad peaks are consistent with the nanoparticles being small (4 nm in diameter) as discussed in

the TEM section before. The lattices are a = 4.738 Å, b = 4.738 Å and c = 3.187 Å. The peaks corresponding to the identification of the cassiterite-type SnO_2 are shown with the green round markers with their indexes. The XRD traces of the CNTs/MnO_2 60% w.t. nanocomposite show the peaks which correspond to monoclinic birnessite-type MnO_2 (JCPDS 42-1317) with lattices of a = 5.150 Å, b = 2.844 Å and c = 7.159 Å. There are three peaks from the acid-treated CNTs as indicated by the yellow triangular markers. The XRD patterns of the CNTs/SnO_2, CNTs/MnO_2, and acid-treated CNTs are presented in Figure 5.

MnO_2 and CNTs are complementary in properties where the three-dimensional structure of their nanocomposite, due to the presence of CNT [21], provides the mesoporous cavity for ion movements. MnO_2 is also known for its low cost and large pseudo-capacitance but has the disadvantage of being resistive [22]. Thus, a nano-layer of MnO_2 on CNT would improve the ion conduction in the MnO_2 phase [10]. The same improvement can be deduced for the CNTs/SnO_2 60% w.t. nanocomposite although SnO_2 is more conducting than MnO_2 (10^2 ~ 10^3 S/cm for SnO_2 vs. 10 ~ 10^2 S/cm for MnO_2) [23-24].

Sn has two stable valences, Sn(IV) and Sn(II), which is the basis for the redox chemistry of solid SnO_2. Thus, the charge storage mechanism for the transition metal oxides was applied to SnO_2 at positive potentials in a recent study [6]. However, no study has reported on using SnO_2 as the negative electrode in supercapacitors. To fill in this gap, the CNTs/SnO_2 nanocomposite was further studied by cyclic voltammetry at different potential ranges. The cyclic voltammogram recorded in a wide potential range, i.e. -0.8 to 0.9 V (vs. Ag/AgCl), is fairly rectangular in the overall shape, although a broad oxidation and reduction peak couple appears around 0.10 V. The peak currents varied linearly with the scan rates. These features are strong evidence of the same electrode reaction being responsible for the current flow in the tested potential range, which is in agreement with the behaviour of pseudo-capacitive materials.

When the potential range was narrowed to only positive or only negative potentials, the recorded cyclic voltammograms retained the respective partial features of the cyclic voltammogram recorded in the wide potential range. The capacitance values derived from the cyclic voltammograms in both positive and negative regions were very much the same, which again is evidence of the same electrode reaction being responsible for the pseudo-capacitance of SnO_2 in the wide potential range of 1.7 V as shown in Figure 6. It is worth pointing out that the cyclic voltammograms in Figure 6 suggest the possibility of using the CNTs/SnO_2 to make a symmetrical 1.7 V supercapacitor. However, because the specific capacitance of CNTs/SnO_2 is only about half of that of CNTs/MnO_2, it was decided to use the latter as positive electrode in the asymmetric supercapacitor.

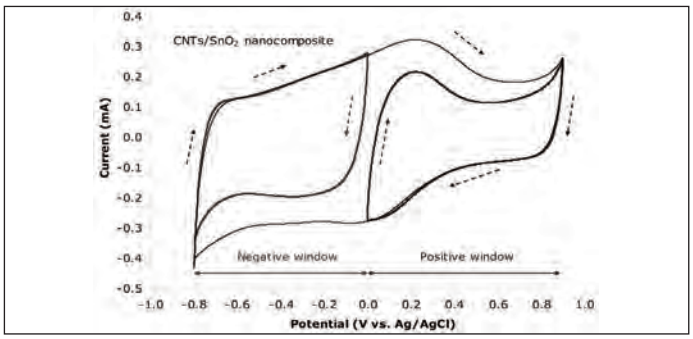

Figure 6: Cyclic voltammograms of the CNTs/SnO_2 in 2.0 M KCl recorded in different potential ranges

Summarising the relevant literature [5, 6] and the aforementioned findings from this work, the charge storage mechanism of the CNTs/SnO_2 nanocomposite can be expressed as equations (2), (3), and (4) below;

Oxidation:

$$Sn(IV)_{(x+y)}OOK_xH_y \rightarrow Sn(IV)O_2 + xK^+ + yH^+ + (x+y)e^- \quad (2)$$

Reduction:

$$Sn(IV)O_2 + xK^+ + yH^+ + (x+y)e^- \rightarrow Sn(IV)_{(x+y)}OOK_xH_y \quad (3)$$

Redox:

$$SnO_2 + xK^+ + yH^+ + (x+y)e^- \rightleftharpoons SnOOK_xH_y \quad (4)$$

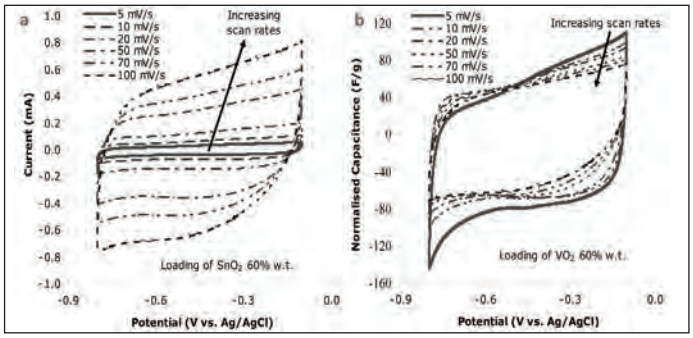

Figure 7: Cyclic voltammograms and mass-normalised capacitance vs. potential (vs. Ag/AgCl) of the CNTs/SnO_2 60% w.t. nanocomposite at various scan rates (5, 10, 20, 50, 70 and 100 mV/s) in 2.0 M KCl. Arrow indicates increasing scan rates

Figure 7 shows the cyclic voltammograms of the CNTs/SnO_2 60% w.t. and its corresponding potential dependent normalised capacitance curves according to $C = \frac{I}{s}$.
The cyclic voltammograms are rectangular and relatively symmetric in current which can be compared with an ideal capacitor. Besides, the increase in the currents of the voltammograms with insignificant changes to their rectangular shapes with increasing scan rate also shows the good electrochemical properties of the nanocomposites and a high rate capability of charge-discharge of the nanocomposite. Figure 7(b) depicts the increase in the mass specific capacitance which is calculated using equation $C = \frac{I}{s}$ with respect to the decrease in scan rate and is in line with the slow response of the mass transfer process in fast scan rates, where ions have limited time to move in and out of the pores of the nanocomposites. It is also interesting to note that the negative ends of the potential windows of the cyclic voltammograms of the CNTs/SnO_2 nanocomposite at various scan rates reach a potential of -0.8 V (vs. Ag/AgCl). This is more negative than the current onset potential (ca. -0.5 V) for hydrogen evolution as observed on the cyclic voltammogram of a platinum electrode in the same aqueous electrolyte. This is indicative of overpotential for hydrogen evolution on the CNTs/SnO_2 electrodes.

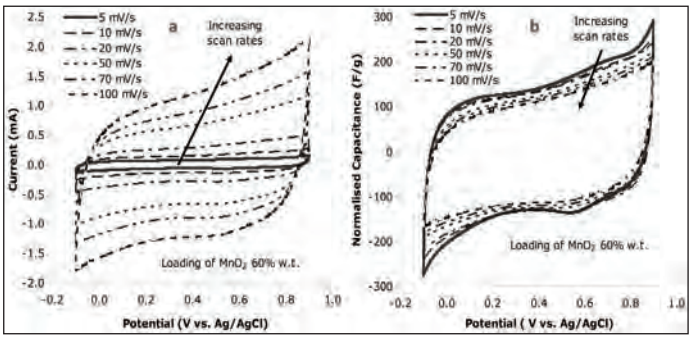

Figure 8: Cyclic voltammograms and mass-normalised capacitance vs. potential (vs. Ag/AgCl) of the CNTs/MnO_2 60% w.t. nanocomposite at various scan rates (5, 10, 20, 50, 70 and 100 mV/s) in 2.0 M KCl. Arrow indicates increasing scan rates. Mass of the CNTs/MnO_2 60% w.t. nanocomposite on the electrode: 0.10 mg

Figure 8 shows the cyclic voltammograms and the corresponding potential dependent normalised capacitance of the CNTs/MnO_2 60% w.t. nanocomposite at different scan rates. The arrows in the figures indicate the direction of the current change with increasing scan rate. The cyclic voltammograms grow larger with increasing scan rate. Even at a fast scan rate of 100 mV/s, the nanocomposite still shows a relatively rectangular cyclic voltammogram, indicating the high rate capability and high reversibility of the redox reaction of the MnO_2 deposited on the CNTs. The charge storage mechanism of the MnO_2 can be explained with reference to the widely accepted understanding of charge transfer reactions in solid transition metal oxides which are usually semiconductors.

The multiple valences of transition metals, e.g. Mn(IV), Mn(II) and Mn(II), are the thermodynamic reason for their ability to undergo electron transfer reactions. To maintain neutrality upon electron transfer into the solid oxide phase, intercalation and adsorption of either or both protons (H^+) and alkali cations (Li^+, Na^+, or K^+) from the electrolyte is necessary [11]. In the CNTs/MnO_2 60% w.t. electrode, both protons and alkali cations have been found to be involved in the redox transition between M(IV) and Mn(III) [11, 25, 26]. During the positive and negative potential sweeps, reversible oxidation and reduction reactions take place in the MnO_2 explained below in the presence of the K^+ cations and H^+ protons from the 2.0 M KCl in equations (5), (6), and (7) below [11, 19, 27];

Oxidation:

$$Mn(III)_{(x+y)}Mn(IV)_{1-(x+y)}OOK_xH_y \rightarrow Mn(IV)O_2+xK^++yH^++(x+y)e^- \quad (5)$$

Reduction:

$$Mn(IV)O_2+xK^++yH^++(x+y)e^- \rightarrow Mn(III)_{(x+y)}Mn(IV)_{1-(x+y)}OOK_xH_y \quad (6)$$

Redox:

$$MnO_2+xK^++yH^++(x+y)e^- \rightleftharpoons MnOOK_xH_y \quad (7)$$

The variation in the mass specific capacitance of the CNTs/MnO_2 60% w.t. nanocomposite with the scan rate in the potential range of -0.1 to 0.9 V is shown in Figure 8(b). At the lowest scan rate of 5 mV/s, the largest normalised capacitance plot is evident as compared to all the other scan rates. The specific capacitance decreases gradually with the increasing scan rate as can be seen. The decrease in specific capacitance was due to the incomplete mass transport process, thus, the incomplete redox reactions, adsorption/desorption, and intercalation/deintercalation of cations or protons in the higher scan rates. The highest average mass specific capacitance at the scan rate of 5 mV/s can be calculated also, utilising the average charge accumulated in the positive and negative sweep of the cyclic voltammogram and is found to be 138.20 F/g in the defined potential range of -0.1 to 0.9 V. A further examination of the electrochemical properties of the nanocomposite was carried out with the galvanostatic charge-discharge technique, and the results are presented in Figure 9.

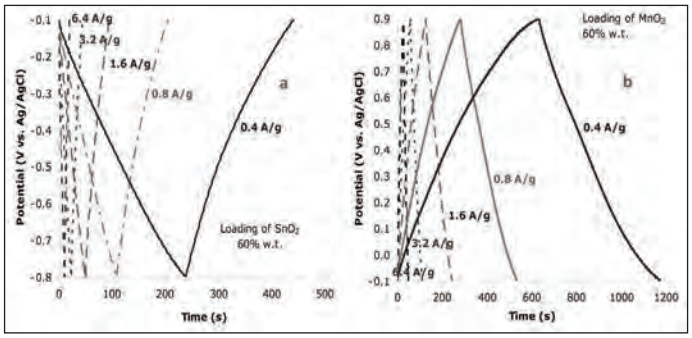

Figure 9: (a) Potential-time plots from the galvanostatic charge-discharge test of the CNTs/SnO_2 60% w.t. nanocomposites and (b) the CNTs/MnO_2 60% w.t. nanocomposites at different normalised currents (0.4, 0.8, 1.6, 3.2, and 6.4 A/g) in 2.0 M KCl

Figure 9(a) shows the potential-time plots from the galvanostatic charge-discharge test of the CNTs/SnO_2 60% w.t. nanocomposites at different normalised currents of 0.4, 0.8, 1.6, 3.2 and 6.4 A/g. The potential-time plot of CNTs/SnO_2 60% w.t. is compared with that of CNTs/VO_2 60% w.t. and the acid-treated CNTs at the normalised current of 0.4 A/g. At the lowest normalised current applied, i.e. 0.4 A/g, a specific capacitance of 130.19 F/g is obtained for the range of -0.8 to -0.1 V against Ag/AgCl. Given that at the same normalised current and potential range, acid-treated CNTs recorded a specific capacitance of 35.11 F/g in the negative range, the specific capacitance of the SnO_2, CM-oxide, assuming proportional contribution can be found to be 193.57 F/g. The potential-time plots from the galvanostatic charge-discharge test of the CNTs/MnO_2 60% w.t. nanocomposite in the Figure 9(b) show linear variation of the potential with respect to time in the potential range of -0.1 to 0.9 V (vs. Ag/AgCl), indicating good capacitive behaviour for all the normalised currents applied, i.e. 0.4, 0.8, 1.6, 3.2 and 6.4 A/g. Even at a higher normalised current of 6.4 A/g, a specific capacitance of 162.00 F/g was recorded for the CNTs/MnO_2 60% w.t. nanocomposite. At the lowest normalised current of 0.4 A/g, the CNTs/MnO_2 60% w.t. nanocomposite registered a capacitance of 236.62 F/g while the acid-treated CNTs recorded a specific capacitance of 41.21 F/g in the positive range. Assuming proportional contribution, the specific capacitance of the MnO_2, $C_{M\text{-}oxide}$ can be determined to be 366.89 F/g.

4.0 CONCLUSION

CNTs/SnO_2 60% w.t. and CNTs/MnO_2 60% w.t. have been successfully synthesised via hydro-oxidation deposition of SnO_2 on the CNTs and reduction of $KMnO_4$ by CNTs i.e. redox and deposition, respectively. The SEM images for the CNTs/SnO_2 revealed jagged surface morphology while the TEM images confirmed the evenly distributed SnO_2 nanoparticulates on the surface of the CNTs throughout the structure. TEM images

validated the existence of uneven coatings MnO_2 on the surface of the CNTs. XRD patterns reveal the presence of SnO_2 (JCPDS 41-1445) and birnessite-MnO_2 (JCPDS 42-1317) in the CNTs/SnO_2 and CNTs/MnO_2 nanocomposites, respectively. CNTs/SnO_2 exhibited an overpotential for hydrogen evolution as no gas evolution was observed for a potential as negative as -0.8 V (vs. Ag/AgCl) while the CNTs/MnO_2 showed an oxygen overpotential on the positive range extending above the potential of the evolution of oxygen at 0.6 V (vs. Ag/AgCl). The maximum values of mass specific capacitance achieved by the CNTs/SnO_2 60% w.t. and the CNTs/MnO_2 60% w.t. were 130.19 F/g and 236.62 F/g respectively at the normalised current of 0.4 A/g. These values correspond to the specific capacitance ($C_{M\text{-}oxide}$) of (assuming proportional contribution) 193.57 and 366.89 F/g for SnO_2 and MnO_2 respectively. The knowledge of the capacitance achievable by these nanocomposite materials can be utilised to build desirable supercapacitors of any sizes to be used in the UPS back-up system or possibly replacing diesel standby generators in the case of blackout. Thus, the results reported in this article on these nanocomposite materials show that they are capable of constructing the next generation supercapacitors which is crucial as we face the energy crisis in the present and in the future and when the engineering world needs more efficient yet environmental-friendly energy storage devices. ■

REFERENCES

[1] Wan K., *et al*. (1998). "Tin-based oxide anode for lithium-ion batteries with low irreversible capacity." Journal of Power Sources. 75(1): pp 9-12.

[2] Mohamedi M., *et al*. (2001). "Amorphous tin oxide films: Preparation and characterization as an anode active material for lithium ion batteries." Electrochimica Acta. 46(8): pp 1161-1168.

[3] Yuan L., *et al*. (2006). "Nano-structured spherical porous SnO_2 anodes for lithium-ion batteries." Journal of Power Sources. 159(1): pp345-348.

[4] Mei L., *et al*. (2007). "Core-shell and hollow microspheres composed of tin oxide nanocrystals as anode materials for lithium-ion batteries." Electrochemical and Solid-State Letters, 2007. 10(8): pp K33-K37.

[5] Rajendra P.K. and Miura N. (2004). "Electrochemical synthesis and characterization of nanostructured tin oxide for electrochemical redox supercapacitors." Electrochemistry Communications. 6(8): pp 849-852.

[6] Wu M., *et al*. (2008). Cathodic deposition and characterization of tin oxide coatings on graphite for electrochemical supercapacitors. Journal of Power Sources. 175(1): pp 669-674.

[7] Wang Z., Chen G., and Xia D. (2008) "Coating of multi-walled carbon nanotube with SnO_2 films of controlled thickness and its application for Li-ion battery." Journal of Power Sources. 184(2): pp 432-436.

[8] Xie J. and Varadan V.K. (2005). "Synthesis and characterization of high surface area tin oxide/functionalized carbon nanotubes composite as anode materials." Materials Chemistry and Physics. 91(2-3): pp 274-280.

[9] Du N., *et al*. (2009). "Synthesis of polycrystalline SnO_2 nanotubes on carbon nanotube template for anode material of lithium-ion battery." Materials Research Bulletin. 44(1): pp 211-215.

[10] Jin X., *et al*. (2007). "Nanoscale microelectrochemical cells on carbon nanotubes." Small. 3(9): pp 1513-1517.

[11] Wu M., *et al*. (2004). "Redox deposition of manganese oxide on graphite for supercapacitors." Electrochemistry Communications. 6(5): pp 499-504.

[12] Dong X., *et al*. (2006). "MnO_2-embedded-in-mesoporous-carbon-wall structure for use as electrochemical capacitors." The Journal of Physical Chemistry B. 110(12): pp 6015-6019.

[13] Huang X., *et al*. (2007). "Preparation and properties of manganese oxide/carbon composites by reduction of potassium permanganate with acetylene black." Journal of The Electrochemical Society. 154(1): pp A26-A33.

[14] Ma S.B., *et al*. (2007). "Synthesis and characterization of manganese dioxide spontaneously coated on carbon nanotubes." Carbon. 45(2): pp 375-382.

[15] Han W.Q. and Zettl A. (2003). Coating single-walled carbon nanotubes with tin oxide. Nano Letters. 3(5): pp 681-683.

[16] McKeown D.A., *et al*. (1999) "Structure of hydrous ruthenium oxides: Implications for charge storage." The Journal of Physical Chemistry B. 103(23): pp 4825-4832.

[17] Hu C.C. and Tsou T.W. (2002). "Ideal capacitive behavior of hydrous manganese oxide prepared by anodic deposition." Electrochemistry Communications. 4(2): pp 105-109.

[18] Conway B.E. (1991). "Transition from "Supercapacitor" to "Battery" behavior in electrochemical energy storage." Journal of The Electrochemical Society. 138(6): pp 1539-1548.

[19] Hu C.C. and Tsou T.W. (2003). The optimization of specific capacitance of amorphous manganese oxide for electrochemical supercapacitors using experimental strategies. Journal of Power Sources. 115(1): pp 179-186.

[20] Ghaem M., *et al*. (2008). "Charge storage mechanism of sonochemically prepared MnO_2 as supercapacitor electrode: Effects of physisorbed water and proton conduction." Electrochimica Acta. 53(14): pp 4607-4614.

[21] Peng C., *et al*. (2008). "Carbon nanotube and conducting polymer composites for supercapacitors." Progress in Natural Science. 18(7): pp 777-788.

[22] Hashmi S. and Updahyaya H. (2002). "MnO_2-polypyrrole conducting polymer composite electrodes for electrochemical redox supercapacitors." Ionics. 8(3): pp 272-277.

[23] Wu N.L., Han C.Y., and Kuo S.L. (2002). " Enhanced performance of SnO_2 xerogel electrochemical capacitor prepared by novel crystallization process." Journal of Power Sources. 109(2): pp 418-421.

[24] Glicksman R. and Morehouse C.K. (1956). "Resistivity studies of various Leclanché cathode materials." Journal of The Electrochemical Society.103(3): pp 149-153.

[25] Khomenko V., Raymundo-Piñero E., and Béguin F. (2006). "Optimisation of an asymmetric manganese oxide/activated carbon capacitor working at 2 V in aqueous medium." Journal of Power Sources. 153(1): pp 183-190.

[26] Lee H.Y. and Goodenough J.B. (1999). " Supercapacitor behavior with KCl electrolyte." Journal of Solid State Chemistry. 144(1): pp 220-223.

[27] Pourbaix M. (1966). "Atlas of electrochemical equilibria in aqueous solutions." Pergamon Press, New York.

PROFILES

IR. DR NG KOK CHIANG graduated from the University of Western Australia with first class honours in Bachelor of Engineering in Electrical & Electronics and Bachelor of Commerce majoring in Accounting, Investment Finance (Derivatives), and Managerial Accounting. He then furthered his studies to the University of Nottingham, UK and graduated with a PhD in Energy Storage Engineering having worked on nanomaterials and nanocomposites for advanced supercapacitors for renewable energy storage for three and a half years. Ir. Dr Ng Kok Chiang in his course of research and work had liaised with various organisations such as E.ON (Power and Gas), Lockheed Martin, Jaguar/Land Rover (supercapacitors in automotive industry/electric cars), Battelle (lab management and commercialisation), Malaysia Rubber Board (energy management) and MOSTI (Fabrication of Advanced Supercapacitors).

He is currently the Chief Technology Officer with MyBIG Sdn. Bhd. involved in various research and prototyping projects in collaboration with various Malaysian Government Agencies and research bodies. Two of the most prominent solutions founded were the advanced switching mechanism for the Nexcap storage incorporated in the Sunopy solar system to efficient capturing of the energy from the solar power.

DR DANIEL A. JEWELL is a Research Associate in the Department of Materials Science and Metallurgy at the University of Cambridge. He received his MEng degree in Engineering at the University of Nottingham, England, UK, where he also completed his PhD in Engineering on the world renowned FFC-Cambridge Process under the supervision of Professor George Chen, one of the inventors.

Since 2009 he has been the primary researcher on the Chinuka Process at the University of Cambridge in collaboration with Professor Derek Fray and White Mountain Titanium Corporation.

Daniel's primary research focus is titanium extraction, but he is also experienced in the manufacture and testing of supercapacitors, and the electrochemical production of carbon.